

# Humanoid Walking Control Using LQR and ANFIS

Muhammad Auzan <sup>1\*</sup>, Danang Lelono <sup>2</sup>, Andi Dharmawan <sup>3</sup>

<sup>1,2,3</sup> Departement of Computer Science and Electronics, Universitas Gadjah Mada, Yogyakarta, Indonesia

Email: <sup>1</sup> muhammadauzan@ugm.ac.id, <sup>2</sup> danang@ugm.ac.id, <sup>3</sup> andi\_dharmawan@ugm.ac.id

\*Corresponding Author

**Abstract**—Humanoid robots possess remarkable mobility and adaptability for diverse environments. Nonetheless, accurate walking pattern tracking remains challenging, especially when employing the linear quadratic regulator (LQR) due to delays in high-mobility setpoint tracking. We propose a novel control approach to address this limitation by integrating an artificial neuro-fuzzy inference system (ANFIS) with the LQR to enhance pattern tracking. The research contributes to developing a control system that combines LQR and ANFIS to enable humanoid robots to follow various walking patterns with increased precision and efficiency and also the scheme to incorporate LQR and ANFIS. The study involves four experiments: step response, walking phase, static straight walking, and varied straight walking. Each test runs for 5 seconds with a 100-millisecond sampling rate, repeated five times, and employs the Integral Absolute Value (IAE) metric for evaluation. The LQR-ANFIS method exhibits superior performance, achieving a maximum overshoot of 0%, a rise time of 0.3 seconds, a settling time of 0.3 seconds, and a steady-state error of 0% in the step response experiment. The proposed control system also enables stable walking with step periods ranging from 0.15 to 4 seconds and step ranges of 0.05 to 0.03 meters. In conclusion, the integration of ANFIS with the LQR significantly enhances the mobility of humanoid robots, enabling them to navigate diverse environments and accurately track various walking patterns proficiently.

**Keywords**—biped, quintic, walking, pattern, ANFIS

## I. INTRODUCTION

Humanoid robots are known for their high mobility and adaptability to diverse environments, driven by their complex degree of freedom (DOF) and dynamics [1]–[3]. While this abundance of DOF endows humanoid robots with the ability to perform various tasks [4]–[7], it also leads to challenges in controlling their intricate body design, power distribution, motion patterns, and movement algorithms [8]–[11].

Humanoid robots move using synchronized joint rotations to achieve specific positions, resulting in continuous, coordinated movements [12]–[15]. Inverse kinematics determines body coordinate positions and destination coordinates of other limbs by calculating the input angle [16]–[19], while forward kinematics calculates limb and center of mass (COM) coordinates [20]–[22].

Despite advances in generating walking patterns based on COM or ZMP criteria [23], [24], the complex nature of humanoid robots can lead to discrepancies between generated

patterns and actual responses. Control systems are crucial for accurate trajectory tracking and overcoming discrepancies [25]–[27], with deterministic methods like Proportional Integral Derivative (PID) and Linear Quadratic Regulator (LQR) commonly employed [28]–[30].

These methods have encouraged various studies that have succeeded in realizing stable humanoid robots with COM and ZMP criteria as the popular criteria [31]–[33]. Based on the COM criteria, the robot moves stably if the COM of the robot is inside the support polygon or within the isolated area [8], [34]. A support polygon is formed by the robot's body touching the ground. In a walking humanoid robot, a support polygon is an area where the sole steps on the ground and forms a shape [35], [36]. Meanwhile, the ZMP criteria state that the robot is stable when the ZMP position of the robot is in polygon support. The ZMP criteria mean that even if the COM of the robot is outside the support polygon, as long as the ZMP is inside the support polygon, the robot will remain stable [37], [38]. These criteria are proven to make robots walk straight in a flat plane [39], [40].

The control system maintains the robot states, for example, the COM and ZMP position, based on the states' error calculated from the system feedback [41]–[43]. Various control systems that have been widely introduced include Proportional Integral Derivative (PID) and Linear Quadratic Regulator (LQR), a linear control system [28]–[30]. PID is a control system that has been long and robust track record. However, PID only processes a system with a single input and output [44], [45]. Meanwhile, humanoid robots are multiple-input, multiple-output (MIMO) systems. Therefore, the LQR control system is more appropriate to process the humanoid robot system [46]–[48].

In addition to deterministic methods, stochastic approaches like Fuzzy control have been explored [49]–[51], but these often rely on expert knowledge for constructing membership functions, leading to varying configurations [52]. The Adaptive Neuro-Fuzzy Inference System (ANFIS) was developed to overcome this limitation [53], [54], employing inverse training to model dynamic systems with finite errors [55], [56]. The stochastic methods give a more nonlinear response than the deterministic methods.

To enhance the control performance of humanoid robots, we



propose a novel approach that integrates full-state feedback LQR and ANFIS control, leveraging LQR simulation to train ANFIS for minimal error production. Serving as an additional controller, ANFIS contributes to improved system action. The research contribution lies in the fusion of LQR and ANFIS for humanoid robot control, and we validate the effectiveness of our method through Coppelia robotic simulation and transient response analysis. First, The research will present our combined LQR and ANFIS approach, which addresses humanoid robot mobility and walking pattern tracking challenges, leading to enhanced control performance. Second, the validation of our proposed method demonstrates its efficacy and applicability in real-world robotic simulations.

## II. METHODS

This research is systematically divided into several stages to ensure a well-structured and purposeful approach as in Fig. 1. The study begins with modeling the robot using a cart table to simplify the humanoid robot representation, where mechanical parameters are derived from Autodesk Inventor designs. Control system modeling is then conducted to obtain state space equations, determine  $K$  values through the LQR method, and collect data sets for ANFIS training. In addition to full-state feedback, ANFIS controls are designed with three inputs and three membership functions. The simulation stage involves tuning  $Q$  and  $R$  components to obtain optimal  $K$  values and gather data for ANFIS training. The research also focuses on designing algorithms to enable humanoid robots to walk in all directions, considering each robot step's final position as input. Control system tests are conducted in real-time on humanoid robots and through simulations using VREP software, analyzing various system responses such as overshoot, steady-state error, rise time, settling time, and integral absolute error (IAE).

### A. Control Framework

The humanoid robot control system receives walking trajectory as the inputs in the shape of continuous position, velocity, and acceleration in the  $x$ ,  $y$ , and  $z$ -axis. The walking trajectory, generated by the quintic polynomial, is converted into ZMP using the cart table model. As such, there are four outputs from the walking trajectory: the robot ZMP value, the robot COM position value, the robot COM velocity value, and the robot COM acceleration value. The ANFIS and full-state feedback control systems need those outputs to calculate the robot's action.

The full-state feedback control system with ANFIS as an additional controller generates the controlled ZMP position in the  $x$  and  $y$ -axis based on the error of robot COM position, COM velocity, and ZMP position in the  $x$  and  $y$ -axis. The error was calculated from the difference between the output of the walking pattern generator and the sensor value, which

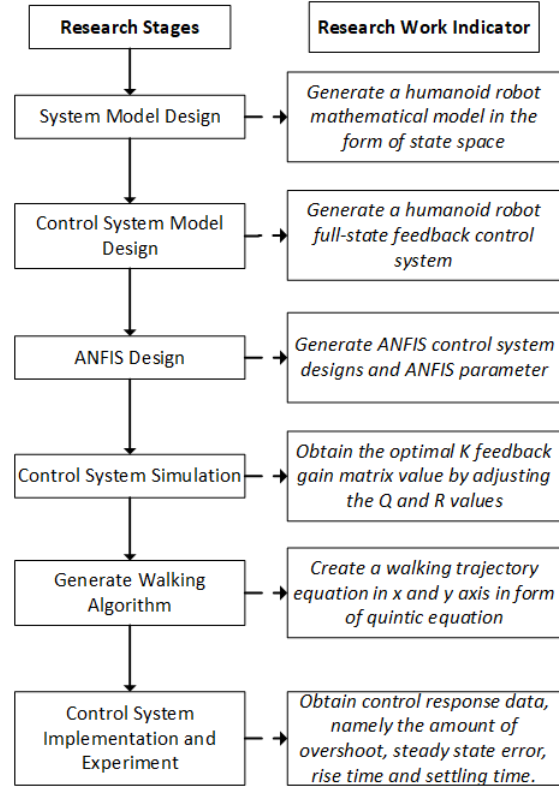


Fig. 1. Research Flow Diagram

was processed using inverse kinematic and cart-table models. The rotary sensor measures every robot's joint position and calculates the robot's actual COM and ZMP using forward kinematics.

The control system then subtracts the generated ZMP reference value from the walking generator and the controlled ZMP value of ANFIS and full-state feedback control to calculate the ZMP for the robot action. The outline of the proposed humanoid robot system is explained in Fig. 2.

Based on the control system framework, five parts are designed to create the walking robot system: a robot model using the cart-table model, a walking pattern generator to generate the ZMP and COM reference, an ANFIS control system for the stochastic control system, and a full-state feedback control system for the deterministic control system.

### B. Cart-Table Model

This research humanoid robot is modeled with a cart-table model. The cart-table model is used so that the ZMP components of the robot can be analyzed and used to improve stability when walking. A humanoid robot modeled with a cart-table model is shown in Fig. 3.

The mathematical equation of the cart-table model is shown

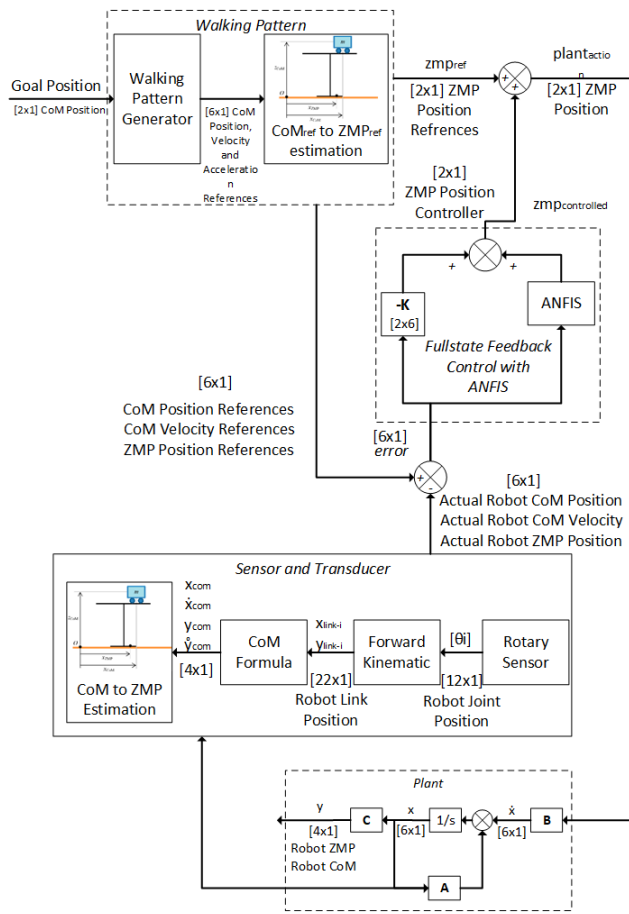


Fig. 2. Humanoid Robot Control Framework

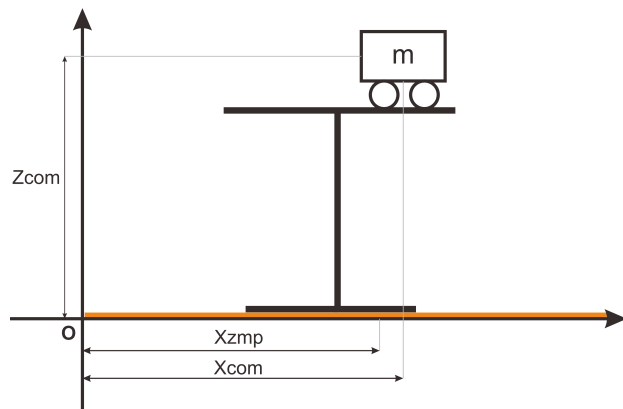


Fig. 3. Cart-Table Model

in (1) and (2). The equation shows that the position of ZMP is affected by the position of COM and also the acceleration of COM.

$$p_x = x - \frac{z}{g} \ddot{x} \tag{1}$$

$$p_y = y - \frac{z}{g} \ddot{y} \tag{2}$$

where  $p_i$  is ZMP position in  $i$  axes (m),  $x$  is COM position in  $x$  axes (m),  $y$  is COM position in  $y$  axes (m),  $z$  is Constant COM position in  $z$  axes (m),  $\ddot{x}$  is COM acceleration in  $x$ -axes ( $m/s^2$ ),  $\ddot{y}$  is COM acceleration in  $y$ -axes ( $m/s^2$ ),  $g$  is gravitational acceleration ( $9.81 m/s^2$ ).

The ZMP approximation can be obtained by first calculating the COM position and COM acceleration value [57]. The position values are obtained from the forward kinematics calculation of each robot joint sensor and then differentiating it to get the COM acceleration value. The ZMP result of (1) and (2) is called the actual ZMP in this work.

### C. Quintic Polynomial Walking Pattern Generator

The walking scheme is divided into five parts; the first is the initial position in the double support phase. The second part is the double support phase, which moves the COM position to the stance leg. The third part is the swing-up phase in the single support phase. The fourth part is the swing-down phase in the single support phase, and the last is the stabilizing phase. The swing-up phase move when the COM position is already in the support polygon region, so the swing-up phase will not wait for the first phase to end. The walking scheme used in this work is shown in Fig. 4 for the sagittal plane and Fig. 5 for the frontal plane.

Quintic polynomials in this system generate the body reference trajectory [58]. The method produces the position, velocity, and acceleration as in (3), (4), and (5).

$$p = b_0 + b_1 t + b_2 t^2 + b_3 t^3 + b_4 t^4 + b_5 t^5 \tag{3}$$

$$v = b_1 + 2b_2 t + 3b_3 t^2 + 4b_4 t^3 + 5b_5 t^4 \tag{4}$$

$$a = 2b_2 + 6b_3 t + 12b_4 t^2 + 20b_5 t^3 \tag{5}$$

To get the variable, use this equation

$$b_0 = p_0 \tag{6}$$

$$b_1 = v_0 \tag{7}$$

$$b_2 = \frac{a_0}{2} \tag{8}$$

$$b_3 = \frac{(20h - (8v_t + 12v_0)T - (3a_0 - a_t)T^2)}{2T^3} \tag{9}$$

$$b_4 = \frac{(-30h + (14v_t + 16v_0)T - (3a_0 - 2a_t)T^2)}{2T^4} \tag{10}$$

$$b_5 = \frac{12h + 6(v_t + v_0)T - (a_t - a_0)T^2}{2T^5} \tag{11}$$

where the variable is  $p_0$  is Initial position,  $p_t$  is Goal Position,  $v_0$  is Initial Velocity,  $v_t$  is Goal Velocity,  $a_0$  is Initial Acceleration,  $a_t$  is Goal Acceleration and  $T$  is Stepping time.

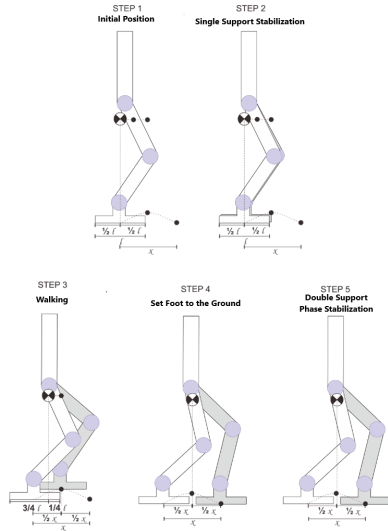


Fig. 4. Proposed walking scheme in the sagittal plane

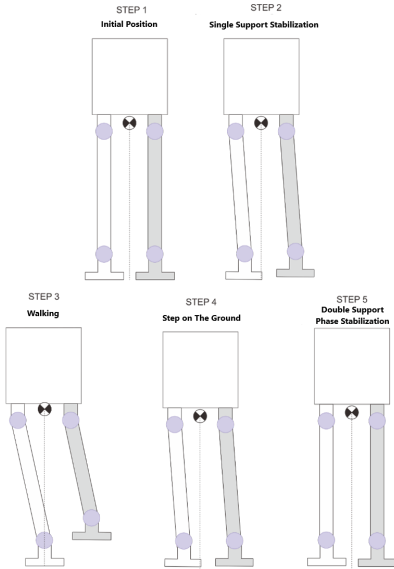


Fig. 5. Proposed walking scheme in the frontal plane

D. ANFIS Control System

ANFIS architecture used in this work is adopted from Sugeno fuzzy inference system [59]. Each controlled axis has one ANFIS control system. Because the controlled axis is the  $x$  and  $y$ , there are two ANFIS designs. There are three inputs in ANFIS: COM error, COM velocity error, and ZMP error. Every input has three membership functions, with every membership function being Gaussian. Using the configuration shown in

Table I, the total number of rules is 27. The overall ANFIS network is shown in Fig. 6.

TABLE I  
ANFIS CONFIGURATION

No	Parameter	Value
1	Fuzzy Inference System	Sugeno
2	AND Methods	Product
3	OR Methods	Max
4	Defuzzification	Weight Average
5	Implication	Product
6	Aggregation	Addition
7	Membership Function	Gaussian

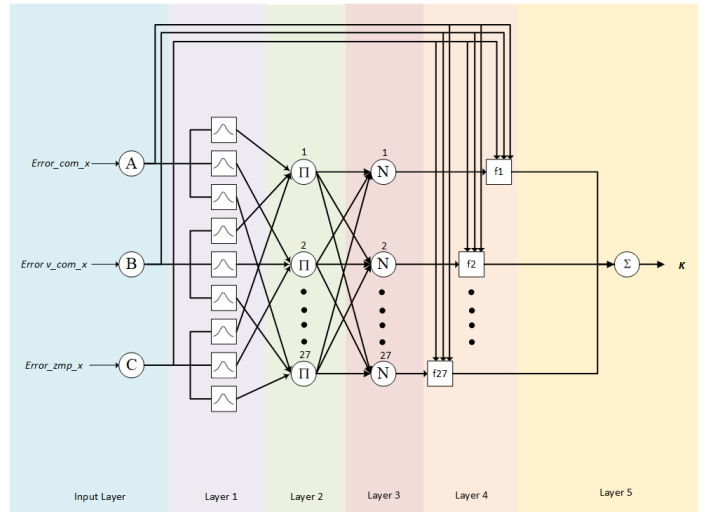


Fig. 6. ANFIS Architecture

The Gaussian membership function is explained in a mathematical formula in (12).

$$\mu(x) = e^{-\frac{1}{2} \left( \frac{x-c}{\sigma} \right)^2} \tag{12}$$

where  $\mu$  is membership value,  $c$  is Gaussian function center,  $\sigma$  is Gaussian function standard deviation, and  $x$  is measured value.

The defuzzification uses weighted average with formula in (13), weight formula in (14), and the rule value formula in (15). ANFIS training will obtain the constant in (15).

$$O = \frac{\sum f_i \cdot w_i}{\sum w_i} \tag{13}$$

$$w_i = \mu_{1i}(x_1) \cdot \mu_{2i}(x_2) \cdot \mu_{3i}(x_3), \quad i = 1, 2, 3 \tag{14}$$

$$f_i = x_1 a_i + x_2 b_i + x_3 c_i + d_i \tag{15}$$

where  $O$  Weighted average output,  $f_i$  is Value of rule  $i$ ,  $w_i$  is Weight of rule  $i$ ,  $\mu_{ji}$  is  $i$  membership value of input  $j$ ,  $x_j$  is Value of input  $j$ , and  $a_i, b_i, c_i, d_i$  is Linear constant for rule  $i$ .

Data used for training are relational data of COM, COM Velocity, and ZMP errors with the system input generated by LQR. The system input was obtained by doing the simulation with a different feedback gain value. The selected gain is the Value that produces a minimum error the proposed data collecting method flowchart shown by Fig. 7.

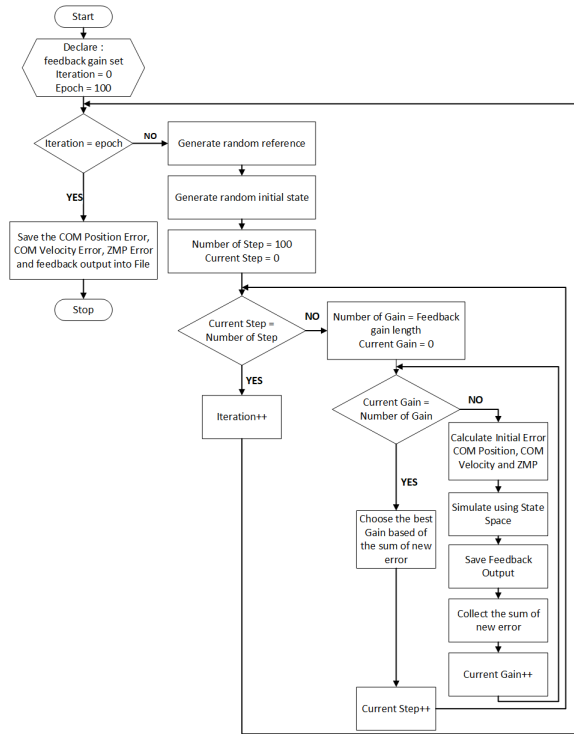


Fig. 7. Proposed Data Collecting Method for ANFIS

The membership function parameter of the proposed ANFIS architecture after training is shown in Table II.

TABLE II  
MEMBERSHIP FUNCTION GAUSSIAN PARAMETER

Membership Function	Range	Linguistic	$\sigma$	$c$
Error COM Position	-9.42 -10.056	Small	4.13	0.316
		Big Negative	4.13	-9.42
		Big Positive	4.13	10.05
Error COM Velocity	-13.901 -16.74	Small	6.507	1.42
		Big Negative	6.507	-13.90
		Big Positive	6.507	16.7
Error ZMP Position	-14.031 -15.38	Small	6.24	0.67
		Big Negative	6.24	-14.03
		Big Positive	6.24	15.3

### E. Full-State Feedback Control System

The humanoid control system used in this work is shown in Fig. 2. The full-state feedback control system has six inputs: COM position, velocity, and ZMP position errors in each  $x$  and

$y$ -axis. As for the full-state feedback control system, the output is two: the ZMP position in the  $x$  and  $y$ -axis. The computed ZMP output is then combined with the ANFIS control system output to get the controller ZMP value.

The plant model used in this work is a model that includes COM and ZMP, which is a cart table model with the formula shown in (1) and (2). The cart-table model is then converted to the state-space model using linearization to obtain the state-space equation [60]. The state space equation of the cart table is shown in (16) and (17).

$$\begin{bmatrix} \dot{x} \\ \dot{x} \\ p_x \\ \dot{y} \\ \dot{y} \\ p_y \end{bmatrix} = \begin{bmatrix} 0 & 1 & 0 & 0 & 0 & 0 \\ \frac{g}{Z_c} & 0 & \frac{-g}{Z_c} & 0 & 0 & 0 \\ 0 & 0 & \frac{-1}{T_p} & 0 & 0 & 0 \\ 0 & 0 & 0 & 0 & 1 & 0 \\ 0 & 0 & 0 & \frac{g}{Z_c} & 0 & \frac{-g}{Z_c} \\ 0 & 0 & 0 & 0 & 0 & \frac{-1}{T_p} \end{bmatrix} \begin{bmatrix} x \\ \dot{x} \\ p_x \\ y \\ \dot{y} \\ p_y \end{bmatrix} + \begin{bmatrix} 0 & 0 \\ 0 & 0 \\ \frac{1}{T_p} & 0 \\ 0 & 0 \\ 0 & 0 \\ 0 & \frac{1}{T_p} \end{bmatrix} \begin{bmatrix} p_x^d \\ p_y^d \end{bmatrix} \quad (16)$$

$$\begin{bmatrix} x \\ p_x \\ y \\ p_y \end{bmatrix} = \begin{bmatrix} 1 & 0 & 0 & 0 & 0 & 0 \\ 0 & 0 & 1 & 0 & 0 & 0 \\ 0 & 0 & 0 & 1 & 0 & 0 \\ 0 & 0 & 0 & 0 & 0 & 1 \end{bmatrix} \begin{bmatrix} \dot{x} \\ p_x \\ y \\ \dot{y} \\ p_y \end{bmatrix} + \begin{bmatrix} 0 & 0 \\ 0 & 0 \end{bmatrix} \begin{bmatrix} p_x^d \\ p_y^d \end{bmatrix} \quad (17)$$

The state spaces of the robot model in (16) and (17) run on MATLAB in continuous and discrete simulation. The continuous simulation would show the natural response of the robot, and the discrete simulation would show the robot's response if controlled with a microcontroller. After the state space model control system is designed, the following steps combine ANFIS and the full-state feedback control by adding each output to enhance each other.

### III. RESULTS AND DISCUSSION

Two experiments are conducted to describe the performance of the proposed method in this work. The first is step response simulation using MATLAB to compare the transient and steady-state response of the LQR and the LQR-ANFIS methods. The second experiment uses CoppeliaSim Edu to investigate the impact of the proposed method on humanoid robot walking ability. The walking period and step length are varied as the robot ability indicator. Integral-absolute-error (IAE) in (18) was used as a performance index and observed in every simulation using CoppeliaSim to describe the tracking performance.

$$IAE = \int_0^T |reference(t) - state(t)| \quad (18)$$

The step response experiment performed using model in (16) and (17) with the following parameter:  $g = 9.81m/s^2$ ,  $Z_c = 0.275m$ , and  $T_p = 0.005s$ . The constant reference used is  $0.1m$  for every input. Full state feedback gain  $K$  used in this work is as follows:

$$K = \begin{bmatrix} -11.0596 & -1.1427 & 1.3418 & 0 & 0 & 0 \\ 0 & 0 & 0 & -11.0596 & -1.1427 & 1.3418 \end{bmatrix} \quad (19)$$

The experiment observes the LQR, ANFIS, and LQR-ANFIS transient and steady-state responses in the  $x$  coordinate, as shown in Fig. 8.

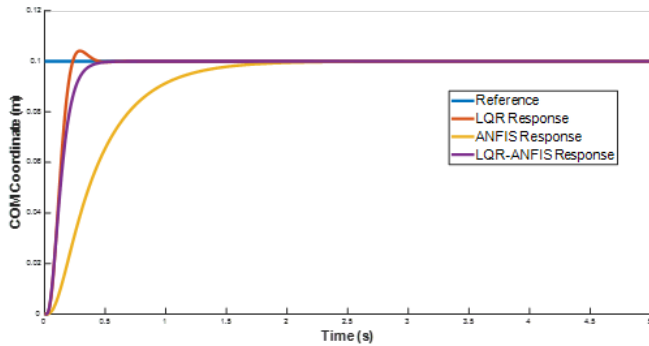


Fig. 8. Comparison of COM Position response in  $x$  coordinate using LQR method, ANFIS method, and LQR-ANFIS method

Step response using LQR feedback gain in 19 gives us a response with a rise time of 0.21 s, settling time of 0.44 s, and 0% steady-state error. However, there is a 4.1% overshoot generated. The 4.1% overshoot is a problem if there is an external force or mechanical error. The LQR-ANFIS method gives us a response with a 0% overshoot compared with LQR-only method. By adding ANFIS, the proposed method has a 0.3 seconds rise time, a settling time of 0.3 seconds, 0% overshoot, and 0% steady-state error.

The result in this stage is a simulation result where no external disturbance affects the robot and does not tell if the robot is falling or failing at walking. Even though there is no disturbance, the LQR-only experiment gives 4.1% overshoot, whereas if we calculate the overshoot using the distance between two legs, 0.0782 meters, gives 0.0032 meters of overshoot. The value is still within the support polygon area, where the area margin is 0.039 meters. The result is also in line with [61] research, where even though there is an overshoot, the humanoid robots can still perform static walking without falling. But, our hypothesis, if external force occurs, such as a leg swing when walking, this overshoot will increase and make a robot fall. Moreover, the LQR response shows us a response that linear with feedback. Feedback gain in (19) indicates that the COM position is more important than the two others, which makes LQR response indices overshoot.

As for the LQR-ANFIS result, 0% overshoot is what this research is after. This result was achieved because the ANFIS can change its feedback priority to adapt to a calculated state. ANFIS calculates new input based on which state has the highest error and prioritizes minimizing it, unlike LQR, which has constant priority over time. ANFIS also changes the full-state feedback characteristic, where the response will be the same in any condition. With additional ANFIS, the response also changes based on the behavior information given

to the fuzzy, where the designed ANFIS architecture here is to minimize the overshoot while speedup the time response. These results are consistent with the study’s initial hypothesis that merging the two methods will reduce errors, as shown in Table III.

TABLE III  
SIMULATION RESULT

Methods	System Respose	Value
LQR	Maximum Overshoot	4.1%
	Risetime	0.21 second
	Settling Time	0.44 second
ANFIS	Maximum Overshoot	0%
	Risetime	1.2 second
	Settling Time	1.53 second
LQR-ANFIS	Maximum Overshoot	0%
	Risetime	0.3 second
	Settling Time	0.3 second

The simulation results in this study illustrate the response characteristics of the control system under a controlled and modeled environment. Although the LQR-only overshoot was within the robot’s support polygon area and static walking was successful, the concern arises regarding potential instability under external forces. On the other hand, the integration of ANFIS with full-state feedback in the LQR-ANFIS method resulted in a desirable 0% overshoot and comparable rise and settling times of 0.3 seconds, while maintaining 0% steady-state error. ANFIS’s ability to adapt its feedback priority dynamically played a crucial role in achieving this improved performance. The findings supported the hypothesis that combining LQR and ANFIS would lead to reduced errors and enhanced tracking performance for humanoid robots during walking tasks. The proposed method offers a promising approach to enhance the control system of humanoid robots and overcome potential challenges during walking, setting a direction for the next experiment in this work.

The second experiment in this work is a simulation using CoppeliaSim and actual robot parameters and models. The engine used in the simulation is a Newton engine with a time sample of 0.1s. The humanoid robot model used in this simulation is a robot with 12 DOF legs shown in Fig. 9.

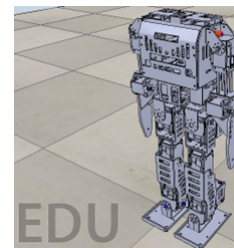


Fig. 9. Humanoid Robot Simulation Model

The result shows that the LQR-ANFIS has a better IAE performance index in every tested walking pattern with an average

result is 0.471 meters for the LQR result and 0.0707 meters for the LQR-ANFIS result. Humanoid robot walking step happens continuously, and as such, errors if not handled fast enough will accumulate in every walking step. The error accumulation happens also in LQR-only and LQR-ANFIS experiments. Even though the LQR-ANFIS gives us a smaller error, if the smaller step and walking period are compared with the bigger step and walking period with the same number of steps, there will be an increase in the IAE value. It also concludes that the error of the proposed method will increase when the walking period and step length increase. As such there is a range where the robot is able to walk safely without falling. The results of the two methods, which were done successfully without falling, are shown in Table IV.

TABLE IV  
WALKING SIMULATION IAE COMPARISON

Walking Period	Step Length	LQR-ANFIS IAE	LQR IAE
2 Second	0.005m	0.457	0.0751
	0.01m	0.787	0.0834
	0.015m	0.563	0.0886
	0.02m	0.631	0.1012
	0.025m	0.689	0.1085
	0.03m	0.747	0.1168
1.5 Second	0.005m	0.235	0.0350
	0.01m	0.266	0.0384
	0.015m	0.277	0.0442
	0.02m	0.313	0.0483
	0.025m	0.329	0.0523
	0.03m	0.358	0.0566

The fewer IAE means that the control system has better performance tracking a different reference in every unit. The LQR-ANFIS can do that because the ANFIS follows the rule where the main priority is to reduce the error first before overcoming the overshoot. Full-state feedback generates system input to overcome the error. However, it cannot reach the reference in one unit of time. However, the ANFIS controller reinforces the generated system input by giving additional input to overcome that error, so the system moves closer to the reference in a one-time unit.

The result of conducted works proves the initial hypothesis that adding an ANFIS that can adapt to the condition will improve the performance of humanoid robot walking. Even though the system response becomes slower than the LQR method, adding an ANFIS aims to improve the tracking performance of a walking humanoid robot. Improvement in tracking performance means the robot can move closer to the given walking pattern.

#### IV. CONCLUSION

ANFIS, as an additional controller in full-state feedback control, can decrease the full-state feedback overshoot but slower response time. The proposed method also achieves better tracking performance of a humanoid robot simulation when

walking using IAE as the comparison value. Better tracking performance means the robot can move closer to the desired walking pattern and overcome disturbances when walking. While our study has shown promising results in enhancing humanoid robot control, there are several aspects for future research. One of them is exploring adaptive control strategies that dynamically adjust the ANFIS parameters during robot locomotion might address the trade-off between response time and overshoot, potentially achieving a faster response without compromising stability.

#### REFERENCES

- [1] D. Wang, Z. Wang, Y. Chen, Z. Cui, Y. Zhu, and C. Wu, "Kinematics analysis and calibration of a 6-degree of freedom light load collaborative robot," *Cobot*, vol. 1, p. 18, 2022.
- [2] Q. Li, F. Meng, Z. Yu, X. Chen, and Q. Huang, "Dynamic Torso Compliance Control for Standing and Walking Balance of Position-Controlled Humanoid Robots," *IEEE/ASME Transactions on Mechatronics*, vol. 26, no. 2, pp. 679–688, 2021.
- [3] X. Zhang, D. You, Z. Yang, Y. Zeng, X. Ai, and S. Wang, "Dimension reduction of inverse kinematics of seven-degree-of-freedom manipulator based on pose separation method," in *2021 4th World Conference on Mechanical Engineering and Intelligent Manufacturing (WCMEIM)*, 2021, pp. 1–5.
- [4] A. Khadidos, "A Comprehensive Study on Robots in Health and Social Care," in *Emerging Technologies in Data Mining and Information Security*. Springer Nature Singapore, 2023, pp. 515–525.
- [5] R. Cisneros, M. Benallegue, M. Morisawa, and F. Kanehiro, "QP-based task-space hybrid / parallel control for multi-contact motion in a torque-controlled humanoid robot," in *2019 IEEE-RAS 19th International Conference on Humanoid Robots (Humanoids)*, 2019, pp. 663–670.
- [6] Z. A. Barakeh, S. Alkork, A. S. Karar, S. Said, and T. Beyrouthy, "Pepper Humanoid Robot as a Service Robot: a Customer Approach," in *2019 3rd International Conference on Bio-engineering for Smart Technologies (BioSMART)*, 2019, pp. 1–4.
- [7] A. Bolotnikova, P. Gergondet, A. Tanguy, S. Courtois, and A. Kheddar, "Task-Space Control Interface for SoftBank Humanoid Robots and its Human-Robot Interaction Applications," in *2021 IEEE/SICE International Symposium on System Integration (SII)*, 2021, pp. 560–565.
- [8] P. Shamma, N. Priya, and K. S. Ahamed, "Walking stability control of biped robot based on three mass with angular momentum model using predictive PID control," in *Proceedings of the International Conference on Electronics, Communication and Aerospace Technology, ICECA 2017*, vol. 2017, 2017, pp. 584–588.
- [9] I. Moskvina, R. Lavrenov, E. Magid, and M. Svinin, "Modelling a Crawler Robot Using Wheels as Pseudo-Tracks: Model Complexity vs Performance," in *2020 IEEE 7th International Conference on Industrial Engineering and Applications (ICIEA)*, 2020, pp. 1–5.
- [10] S. N. Aslan, A. Ucar, and C. Guzelis, "Development of Deep Learning Algorithm for Humanoid Robots to Walk to the Target Using Semantic Segmentation and Deep Q Network," in *2020 Innovations in Intelligent Systems and Applications Conference (ASYU)*, 2020, pp. 1–6.
- [11] S. Sherif and V. Kanchev, "Identification of Humanoid Biped Robot During Walking with Linear Regression Models," in *2019 22nd International Conference on Process Control (PC19)*, 2019, pp. 197–202.
- [12] I. Virgala, L. Miková, T. Kelemenová, M. Varga, R. Rákay, M. Vagaš, J. Semjon, R. Jánoš, M. Sukop, P. Marcinko, and P. Tuleja, "A Non-Anthropomorphic Bipedal Walking Robot with a Vertically Stabilized Base," *Applied Sciences*, no. 9, p. 4108, 2022.
- [13] H. Issa, B. Varga, and J. K. Tar, "Accelerated Reduced Gradient Algorithm for Solving the Inverse Kinematic Task of Redundant Open Kinematic Chains," in *2021 IEEE 15th International Symposium on Applied Computational Intelligence and Informatics (SACI)*, 2021, pp. 000 387–000 392.
- [14] A. J. Valencia, M. Mauleudoux, and C. Castaneda, "Inverse, Direct Kinetics and Differential Kinematic Control of Parallel Robot with Six Degrees of

- Hexa Freedom Hunt,” in *2019 IEEE 10th International Conference on Mechanical and Aerospace Engineering (ICMAE)*, 2019, pp. 563–567.
- [15] H. Issa, B. Varga, and J. K. Tar, “A Receding Horizon-type Solution of the Inverse Kinematic Task of Redundant Robots,” in *2021 IEEE 15th International Symposium on Applied Computational Intelligence and Informatics (SACI)*, 2021, pp. 000 231–000 236.
- [16] C. Jing and J. Zheng, “Improved Algorithm for Solving Inverse Kinematics of Biped Robots,” *Mobile Networks and Applications*, vol. 27, no. 3, pp. 975–983, 2022.
- [17] C. A. My, D. X. Bien, B. H. Tung, L. C. Hieu, N. V. Cong, and T. V. Hieu, “Inverse kinematic control algorithm for a welding robot - positioner system to trace a 3D complex curve,” in *2019 International Conference on Advanced Technologies for Communications (ATC)*, 2019, pp. 319–323.
- [18] A. J. Valencia, M. Mauleodou, and C. Castaneda, “Inverse, Direct Kinetics and Differential Kinematic Control of Parallel Robot with Six Degrees of Hexa Freedom Hunt,” in *2019 IEEE 10th International Conference on Mechanical and Aerospace Engineering (ICMAE)*, 2019, pp. 563–567.
- [19] M. H. Prio and F. Rios, “Kinematic Modeling of a Six Wheeled Differential Drive Intelligent Robot and Potential Field Method to Attain Obstacle Avoidance Capability,” in *2019 SoutheastCon*, 2019, pp. 1–4.
- [20] W. Shenli, L. Xiaoming, L. Ling, and Y. Zimeng, “Bacterial foraging optimization algorithm based on normal cloud model for forward kinematics of a 4-DOF parallel manipulator,” *Ferroelectrics*, vol. 594, no. 1, pp. 175–188, 2022.
- [21] T. Pachidis, C. Sgouros, V. G. Kaburlasos, E. Vrochidou, T. Kalampokas, K. Tziridis, A. Nikolaou, and G. A. Papakostas, “Forward Kinematic Analysis of JACO 2 Robotic Arm Towards Implementing a Grapes Harvesting Robot,” in *2020 International Conference on Software, Telecommunications and Computer Networks (SoftCOM)*, 2020, pp. 1–6.
- [22] Y. Pan, J. Tang, Q. Zhao, and S. Zhu, “Forward and Inverse Kinematics Modeling and Simulation of Six-axis Joint Robot Arm Based on Exponential Product Method,” in *2020 IEEE 3rd International Conference on Automation, Electronics and Electrical Engineering (AUTEEE)*, 2020, pp. 372–375.
- [23] J. Yu, Y. Liu, R. Li, G. Zuo, and N. Yu, “Stable Walking of Seven-link Biped Robot Based on CPG-ZMP Hybrid Control Method,” in *2021 IEEE International Conference on Robotics and Biomimetics (ROBIO)*, 2021, pp. 870–874.
- [24] Y.-C. Wu, H.-W. Lin, and M.-T. Ho, “Gait Planning and Control of a Biped Robot with Walking Pattern Generator and Auxiliary ZMP,” in *2021 International Automatic Control Conference (CACSC)*, 2021, pp. 1–8.
- [25] E. Added and H. Gritli, “Trajectory Design and Tracking-Based Control of the Passive Compass Biped,” in *2020 4th International Conference on Advanced Systems and Emergent Technologies (IC\_ASET)*, 2020, pp. 417–424.
- [26] Q. Huang, C. Dong, Z. Yu, X. Chen, Q. Li, H. Chen, and H. Liu, “Resistant Compliance Control for Biped Robot Inspired by Humanlike Behavior,” *IEEE/ASME Transactions on Mechatronics*, pp. 1–11, 2022.
- [27] K. P. Yadav and R. P. Kumar, “Discrete Feedback Control for Robust Walking of Biped Dynamic Walker,” in *2021 9th International Conference on Control, Mechatronics and Automation (ICMA)*, 2021, pp. 120–123.
- [28] E. S. Varghese, A. K. Vincent, and V. Bagyaveereswaran, “Optimal control of inverted pendulum system using PID controller, LQR and MPC,” *IOP Conference Series: Materials Science and Engineering*, vol. 263, no. 5, 2017.
- [29] R. Ranjan and G. D. Meena, “PID and Backstepping Controller on a 2-Link Biped Robot,” in *2022 2nd International Conference on Emerging Frontiers in Electrical and Electronic Technologies (ICEFEET)*, 2022, pp. 1–6.
- [30] X. T. Nguyen, T. D. Tran, H. H. Nguyen, N. P. Tong, T. P. Nguyen, and T. T. Nguyen, “Controlling Center of Mass in Humanoid Robot using Sliding Mode Control,” in *2020 International Conference on Advanced Mechatronic Systems (ICAMechS)*, 2020, pp. 17–22.
- [31] H. Y. Park, J. H. Kim, and K. Yamamoto, “A New Stability Framework for Trajectory Tracking Control of Biped Walking Robots,” *IEEE Transactions on Industrial Informatics*, vol. 18, no. 10, pp. 6767–6777, oct 2022.
- [32] Z. Wang, K. Harada, and W. Wan, “Multi-contact Stability of Humanoids using ZMP and CWC,” in *2019 IEEE-RAS 19th International Conference on Humanoid Robots (Humanoids)*, 2019, pp. 126–131.
- [33] J. Song and I. Sharf, “Time Optimal Motion Planning with ZMP Stability Constraint for Timber Manipulation,” in *2020 IEEE International Conference on Robotics and Automation (ICRA)*, 2020, pp. 4934–4940.
- [34] M. Kamedula and N. G. Tsagarakis, “Reactive Support Polygon Adaptation for the Hybrid Legged-Wheeled CENTAURO Robot,” *IEEE Robotics and Automation Letters*, vol. 5, no. 2, pp. 1734–1741, 2020.
- [35] S. Xie, X. Li, H. Zhong, C. Hu, and L. Gao, “Compliant Bipedal Walking Based on Variable Spring-Loaded Inverted Pendulum Model with Finite-sized Foot,” in *2021 6th IEEE International Conference on Advanced Robotics and Mechatronics (ICARM)*, 2021, pp. 667–672.
- [36] D. Astudillo, L. I. Minchala, F. Astudillo-Salinas, A. Vazquez-Rodas, and L. Gonzalez, “A simple mapping methodology of gait biomechanics for walking control of a biped robot,” in *2018 IEEE XXV International Conference on Electronics, Electrical Engineering and Computing (INTERCON)*, 2018, pp. 1–4.
- [37] Z. Yu, Q. Zhou, X. Chen, Q. Li, L. Meng, W. Zhang, and Q. Huang, “Disturbance Rejection for Biped Walking Using Zero-Moment Point Variation Based on Body Acceleration,” *IEEE Transactions on Industrial Informatics*, vol. 15, no. 4, pp. 2265–2276, 2019.
- [38] L. Ding, G. Wang, H. Gao, G. Liu, H. Yang, and Z. Deng, “Footstep planning for hexapod robots based on 3d quasi-static equilibrium support region,” *Journal of Intelligent & Robotic Systems*, vol. 103, pp. 1–21, 2021.
- [39] S. Caron, “Biped Stabilization by Linear Feedback of the Variable-Height Inverted Pendulum Model,” in *2020 IEEE International Conference on Robotics and Automation (ICRA)*, 2020, pp. 9782–9788.
- [40] S. Kajita, M. Morisawa, K. Miura, S. Nakaoka, K. Harada, K. Kaneko, F. Kanehiro, and K. Yokoi, “Biped walking stabilization based on linear inverted pendulum tracking,” in *2010 IEEE/RSJ International Conference on Intelligent Robots and Systems*, Taipei, 2010, pp. 4489–4496.
- [41] S. Savin, S. Jatsun, and L. Vorochayeva, “Modification of constrained LQR for control of walking in-pipe robots,” in *2017 Dynamics of Systems, Mechanisms and Machines (Dynamics)*, 2017, pp. 1–6.
- [42] K. Rincon, I. Chairez, and W. Yu, “Finite-Time Output Feedback Robust Controller Based on Tangent Barrier Lyapunov Function for Restricted State Space for Biped Robot,” *IEEE Transactions on Systems, Man, and Cybernetics: Systems*, vol. 52, no. 8, pp. 5042–5055, 2022.
- [43] W. Znegui, H. Gritli, and S. Belghith, “Control of the Passive-Dynamic Locomotion of the Compass-Gait Biped Robot,” in *2020 4th International Conference on Advanced Systems and Emergent Technologies (IC\_ASET)*, 2020, pp. 158–165.
- [44] “Single-Input Single-Output System with Multiple Time Delay PID Control Methods for UAV Cluster Multiagent Systems,” *Security and Communication Networks*, vol. 2022, pp. 1–7, 2022.
- [45] R. P. Borase, D. Maghade, S. Sondkar, and S. Pawar, “A review of pid control, tuning methods and applications,” *International Journal of Dynamics and Control*, vol. 9, pp. 818–827, 2021.
- [46] P. Duan, L. He, Z. Duan, and L. Shi, “Distributed Cooperative LQR Design for Multi-Input Linear Systems,” *IEEE Transactions on Control of Network Systems*, pp. 1–12, 2022.
- [47] J. Yu, R. Li, D. Gong, Y. Liu, and P. Liu, “Research on Disturbance of Upright Balance of Biped Humanoid Robot Based on AWPSO-LQR,” in *2021 IEEE International Conference on Robotics and Biomimetics (ROBIO)*, 2021, pp. 907–912.
- [48] M. Mihalec, M. Trkov, and J. Yi, “Recoverability-Based Optimal Control for a Bipedal Walking Model With Foot Slip,” in *2021 American Control Conference (ACC)*, 2021, pp. 1770–1775.
- [49] M. Aatabe, F. El Guezar, H. Bouzahir, and A. N. Vargas, “Constrained stochastic control of positive Takagi-Sugeno fuzzy systems with Markov jumps and its application to a DC-DC boost converter,” *Transactions of the Institute of Measurement and Control*, vol. 42, no. 16, pp. 3234–3242, 2020.
- [50] M. Sobirin and H. Hindersah, “Stability Control for Bipedal Robot in Standing and Walking using Fuzzy Logic Controller,” in *2021 IEEE International Conference on Industry 4.0, Artificial Intelligence, and Communications Technology (IAICT)*, 2021, pp. 1–7.

- [51] L.-F. Wu and T.-H. S. Li, "Fuzzy Dynamic Gait Pattern Generation for Real-Time Push Recovery Control of a Teen-Sized Humanoid Robot," *IEEE Access*, vol. 8, pp. 36 441–36 453, 2020.
- [52] F. Cao and Y. Li, "Fuzzy adaptive nonlinear stochastic control for vehicle suspension with electromagnetic actuator," *Measurement and Control*, vol. 53, no. 7-8, pp. 1364–1375, 2020.
- [53] I. Chawla, V. Chopra, and A. Singla, "Robust LQR Based ANFIS Control of x-z Inverted Pendulum," *Proceedings - 2019 Amity International Conference on Artificial Intelligence, AICAI 2019*, pp. 818–823, 2019.
- [54] D. Karaboga and E. Kaya, "Adaptive network based fuzzy inference system (anfis) training approaches: a comprehensive survey," *Artificial Intelligence Review*, vol. 52, pp. 2263–2293, 2019.
- [55] Y. H. Chen and C. D. Chang, "An intelligent ANFIS controller design for a mobile robot," *Proceedings of 4th IEEE International Conference on Applied System Innovation 2018, ICASI 2018*, no. 1, pp. 445–448, 2018.
- [56] D. Deshmukh, D. K. Pratihari, A. K. Deb, H. Ray, and A. Ghosh, "Anfis-based inverse kinematics and forward dynamics of 3 dof serial manipulator," in *Hybrid Intelligent Systems: 20th International Conference on Hybrid Intelligent Systems (HIS 2020)*, 2021, pp. 144–156.
- [57] N. Scianca, D. De Simone, L. Lanari, and G. Oriolo, "Mpc for humanoid gait generation: Stability and feasibility," *IEEE Transactions on Robotics*, vol. 36, no. 4, pp. 1171–1188, 2020.
- [58] P. Seiwald, F. Sygulla, N.-S. Staufenberg, and D. Rixen, "Quintic spline collocation for real-time biped walking-pattern generation with variable torso height," in *2019 IEEE-RAS 19th International Conference on Humanoid Robots (Humanoids)*, 2019, pp. 56–63.
- [59] I. Aldarraj, A. Kakei, A. G. Ismaeel, G. Tsaramirsis, F. Q. Khan, P. Randhawa, M. Alrammal, and S. Jan, "Takagi-sugeno fuzzy modeling and control for effective robotic manipulator motion," *arXiv preprint arXiv:2112.03006*, 2021.
- [60] G. Zambella, G. Lentini, M. Garabini, G. Grioli, M. G. Catalano, A. Palleschi, L. Pallottino, A. Bicchi, A. Settini, and D. Caporale, "Dynamic whole-body control of unstable wheeled humanoid robots," *IEEE Robotics and Automation Letters*, vol. 4, no. 4, pp. 3489–3496, 2019.
- [61] A. Dharmawan, C. Habiba, and M. Auzan, "Walking stability control system on humanoid when turning based on LQR method," *International Journal of Scientific and Technology Research*, vol. 8, no. 11, pp. 2606–2611, 2019.